Estimating the Center of Mass of a Free-Floating Body in Microgravity

L. Lejeune, P-F. Migeotte *Member, IEEE,* C. Casellato, X. Neyt *Member, IEEE*

***Abstract*—This paper addresses the issue of estimating the position of the center of mass of a free-floating object in microgravity using a stereoscopic system. The considered object is given an initial translational and rotational velocity at the beginning of a parabola and several consecutive frames are recorded. A motion-based method based on rigid body physics is applied to the reconstructed 3D point cloud to estimate the position of the center of mass. For validation purposes, an object of known geometry and mass distribution is considered.**

I. Introduction

MICROGRAVITY provides weightless conditions where, according to rigid body physics, the movement of an object is only composed of a translation and a rotation around its center of mass (CoM), both of constant velocity. This paper constitutes a proof of concept for a motion-based method intended to be used to estimate the position of the CoM of human subjects in microgravity. Experimental data were gathered in parabolic flight using a box-like object of known geometry and mass distribution for validation purposes. The apparatus consists of a stereoscopic system composed of two DSLR cameras. During the microgravity phase, the object is given an initial rotation and left free-floating. During that time several frames are shot. The data is then processed to obtain a moving 3D point cloud, to which the motion-based reconstruction method is applied to estimate the position of the CoM.

II. Protocols and experimental procedures

The experiment was performed during the ESA (European Space Agency) 57th parabolic flight campaign in October 2011. The box-shaped object that was manipulated is shown in figure 1. It's dimensions are $800 \times 200 \times 200\,mm$. Fiducial markers have been placed along its edges to improve the robustness of the 3d reconstruction. The experiment was conducted by two operators strapped on the floor of the airplane. At the beginning of the parabola, the first operator was standing in front of the cameras holding the object in his hands. At the start of the microgravity phase, an initial rotation was given to the object. It was then left free-floating as long as possible. A second operator, standing behind the cameras, triggered them using a remote control. Both cameras shot the scene simultaneously at a fixed frame rate. At the end of the parabola, the object was recovered by the first operator. The procedure was repeated several times.

L. Lejeune, P-F. Migeotte and X. Neyt are with the Vital Signs and Performance (VIPER) research unit of the Royal Military Academy, Brussels, Belgium (email: laurent.lejeune@elec.rma.ac.be). Claudia Casellatoa is with the NearLab of the Politecnico di Milano (email: claudia.casellato@mail.polimi.it)

Fig. 1. Object free-floating during a parabola.

III. Methods

The stereoscopic system is calibrated off-line using the CALtag self-identifying checkerboard [1], combined with a MATLAB implementation of Zhang's calibration algorithm [2]. Figure 2 shows the general framework for the data processing stage. Extracting points of interest on the object is done in a semi-automatic way: For each left/right pair of frames, points are selected manually in the left view. The corresponding point is then found in the right view via epipolar geometry and a simple cross-correlation based method. By triangulating the two corresponding 2D points, the depth is reconstructed. The position of the CoM is then estimated using two methods. The first one (leftmost branch) is based solely on geometrical properties and requires the 3D coordinates of at least three corners of a face. A single pair of frames is needed to reconstruct the CoM. The second method, because it relies on motion, needs several consecutive pair of frames to operate. The two methods are presented in more details in the following section.

A. Geometry-based method

As stated previously, this method only applies for objects of which the geometry and mass distribution is known, providing reference data with which our motion-based method is

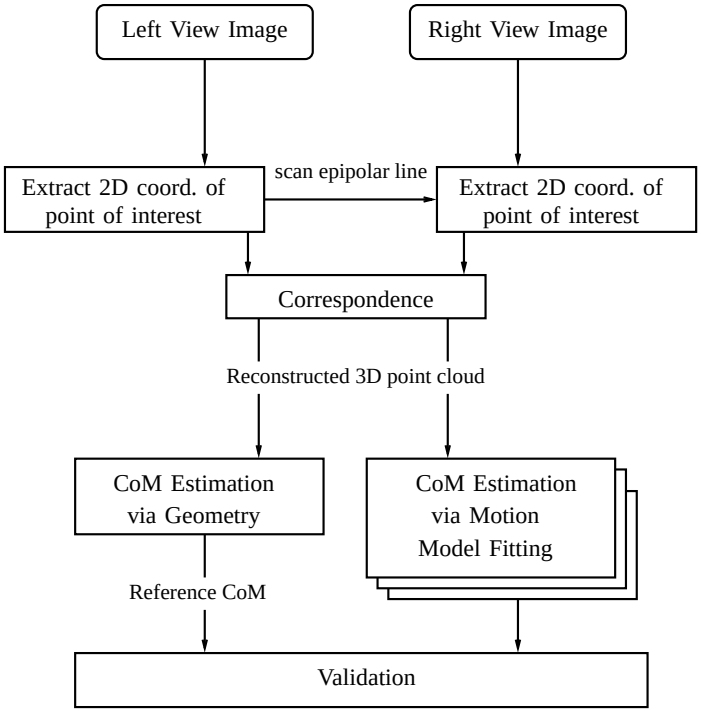

Fig. 2. Framework for the validation of the motion-based method.

evaluated. Determining geometrically the position of the CoM of our object is quite straightforward. Given the coordinates of three corners belonging to the same face M_0, M_1 and M_2, the CoM B is calculated using the face center point M_c and the unitary vector $\boldsymbol{n}$ normal to the considered face (cf. figure 3). In the object reference system $(\boldsymbol{M_0}, \boldsymbol{i_{ob}}, \boldsymbol{j_{ob}}, \boldsymbol{k_{ob}})$, we have:

$$\boldsymbol{B} = \boldsymbol{M_c} + \frac{c}{2}\boldsymbol{n}$$

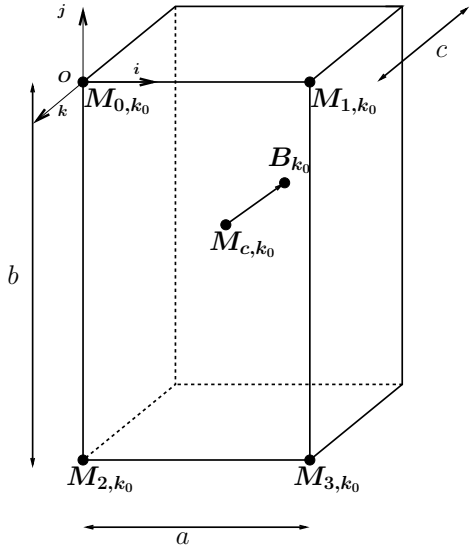

Fig. 3. Box-like object. Four corners are extracted

B. Motion-based method

This method can be applied in the general case where the mass distribution and the geometry of the object is more complex. However, we will see later on that a symmetry plane must be defined. We start by proposing a forward model which, given a point-cloud corresponding to a rigid object and a trajectory (translation and rotation), allows to calculate the coordinates of the point-cloud at later time instants. The goal is then to solve the inverse problem, which can be formulated as follows: Assuming that the motion is governed by the proposed forward model and knowing the coordinates of the point-cloud at several time instants, what is the optimal estimate of the position of the CoM.

1) Forward model: It is assumed that the object is observed in an inertial reference frame. Also, the object is rigid and free-floating, i.e. no external force is applied. According to rigid-body dynamics, its movement is composed of a constant translational velocity and a rotation of constant velocity around its CoM.

We write the 3D N-point cloud at time k: $\{\boldsymbol{M}_{1,k}, ..., \boldsymbol{M}_{N,k}\}$. The associated CoM is denoted $\boldsymbol{B}_k$. The motion depends on the instantaneous translational velocity $\boldsymbol{V}_k$ and rotational velocity $\boldsymbol{\Omega}_k$ which will be referred to by its rotation matrix $\boldsymbol{R}_k$. The time sampling is assumed to be constant, thus, in order to improve readability, both the translational and rotational velocities are normalized with respect to the time sampling frequency. Also, the coordinate of the i-th point at time $k+1$ is given by the following recursive equations:

$$\boldsymbol{B}_k = \boldsymbol{B}_{k-1} + \boldsymbol{V}_{k-1} \tag{1}$$

$$\boldsymbol{M}_{i,k+1} = \boldsymbol{R}_k \left[\boldsymbol{M}_{i,k} - \boldsymbol{B}_k\right] + \boldsymbol{B}_k + \boldsymbol{V}_k \tag{2}$$

$$\tilde{\boldsymbol{M}}_{i,k+1} = \boldsymbol{M}_{i,k+1} + \boldsymbol{w} \tag{3}$$

Where $\boldsymbol{w}$ is a noise vector that accounts for pixel detection error.

Figure 4 illustrates a box-shaped object to which our forward model is applied on two consecutive frames.

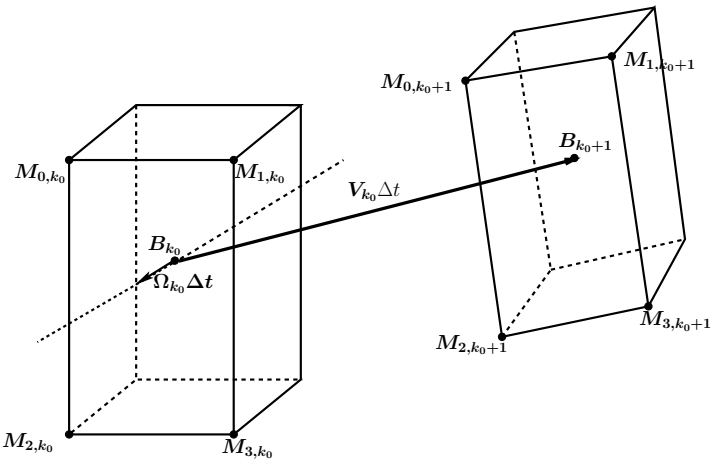

Fig. 4. Applying the forward model to an object.

2) Inverse problem: At time k_0, the inverse problem consists in estimating $\boldsymbol{B}_{k_0}$ from $\{\tilde{\boldsymbol{M}}_{1,k}, ..., \tilde{\boldsymbol{M}}_{N,k}\}$, $k \in [k_0 - \tau; k_0 + \tau]$. Without loss of generality, let's assume for now that the CoM is not moving, i.e. $\boldsymbol{V}_k = 0$, $\forall k$ and $\hat{\boldsymbol{R}}_k$, the estimate of the rotational velocity, is known. The geometric nature of the forward model leads to the inverse problem being ill-posed. Indeed, the position of the CoM, which is such that $d\left(\boldsymbol{M}_{i,k_0}, \boldsymbol{B}_{k_0}\right) = d\left(\boldsymbol{M}_{i,k_{0+1}}, \boldsymbol{B}_{k_0}\right) \quad \forall i$, actually describes the instantaneous axis of rotation. To circumvent this indeterminacy, one needs to provide a constraint. In our application, because the mass distribution of the considered object is symmetrical, the CoM is contained on a symmetry plane. The CoM will thus be defined as the intersection of the instantaneous axis of rotation with the symmetry plane. In what follows, estimation methods for the motion parameters $\boldsymbol{R}$ and $\boldsymbol{V}$ are presented. The CoM will then be estimated over a sequence of point-clouds by assuming that the motion parameters are constant within it.

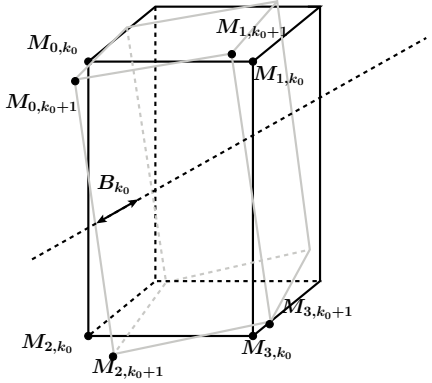

Fig. 5. Ill-conditioned inverse problem.

a) Estimating motion parameters: To perform our estimations , we consider that $\boldsymbol{R}$ and $\boldsymbol{V}$ are constant within the time window corresponding to our point-cloud sequence. This is compatible with the physical assumptions underlying our forward model.

Estimating the rotation of a given sequence has been extensively studied [3] and applied in various fields. We implemented the SVD-based algorithm presented by K. Arun et al. in [4], which allow to estimate, for each pair of consecutive frames, a rotation matrix. The euclidean mean of the matrices was then calculated as explained in [5]. As for the translational velocity, once again, an indetermination appears. Indeed, if we try to eliminate $\boldsymbol{B}_k$ from equation 2 by expressing $\dot{\boldsymbol{M}}_{i,k+1} = \boldsymbol{M}_{i,k+2} - \boldsymbol{M}_{i,k+1}$ in function of $\boldsymbol{R}_k$ and $\boldsymbol{V}_k$, and replacing $\boldsymbol{R}_k$ by its estimate, we notice that the set of solutions correspond to the plane that fits the several consecutive rotation axes of the point-cloud. Our solution consists in replacing $\boldsymbol{B}_k$ by the centroid $\bar{\boldsymbol{M}}_k$ in equation 2, and considering τ past frames and τ future frames. We thus write the mean velocity on a window of length $N_{frames} = 2\tau + 1$ as:

$$\hat{\boldsymbol{V}}_{k_0} = \sum_{i=1}^{N} \sum_{k=k_0-\tau}^{k_0+\tau} \tilde{\boldsymbol{M}}_{i,k+1} - \left(\hat{\boldsymbol{R}}_{k_0}\left(\tilde{\boldsymbol{M}}_{i,k} - \bar{\boldsymbol{M}}_k\right) + \bar{\boldsymbol{M}}_k\right)$$

It can be shown that this estimator is biased but asymptotically unbiased and consistent, i.e. $\hat{\boldsymbol{V}}_{k_0} \to \boldsymbol{V}_{k_0}$ and $E[(\hat{\boldsymbol{V}}_{k_0} - \boldsymbol{V}_{k_0})^2] \to \inf$ as $\tau \to \inf$. Those properties are verified in the simulation section.

b) Least-squares optimization for the CoM: The estimated CoM is now constrained on the symmetry plane. Let $\boldsymbol{P}_{k_0}$ be a point on the symmetry plane and $\boldsymbol{u}, \boldsymbol{v} \in \mathbb{R}^{\not\vDash}$ two non-colinear vectors, we write:

$$\hat{\boldsymbol{B}}_{k_0} = \boldsymbol{P}_{k_0} + \lambda \boldsymbol{u} + \mu \boldsymbol{v} \quad \lambda, \mu \in \mathbb{R}$$

The CoM can now be estimated by solving eq. 2 in the least-squared sense on a window of length $2\tau + 1$:

$$\hat{\boldsymbol{B}}_{k_0,\lambda,\mu} = \arg\min_{\lambda,\mu} \sum_i \sum_{k=k_0-\tau}^{k_0+\tau} \left\| \left(\boldsymbol{I_3} - \hat{\boldsymbol{R}}_{k_0}^{k-k_0}\right) \boldsymbol{B}_{k_0,\lambda,\mu} - \left[\tilde{\boldsymbol{M}}_{i,k} - \left(\hat{\boldsymbol{R}}_{k_0}^{k-k_0} fbm\tilde{M}_{i,k_0} + (k-k_0)\hat{\boldsymbol{V}}_{k_0}\right)\right] \right\|^2 \quad (4)$$

IV. Results

A. Simulations

The performance of the motion-based method is now evaluated through simulation. Based on a set of experimental data, typical values of parameters $\boldsymbol{V}$ and $\boldsymbol{R}$ are chosen. The space coordinates of the box-like object of figure 3 are generated using its actual dimensions. The moving point-cloud is then obtained by applying the forward model at a frame rate of $5fps$. Uniform noise is then added. For several number of frames, 200 runs are generated. The reconstruction error $\epsilon = \left\| \hat{\boldsymbol{B}}_{k_0} - \boldsymbol{B}_{k_0} \right\|$ is computed along with the mean and standard deviation.

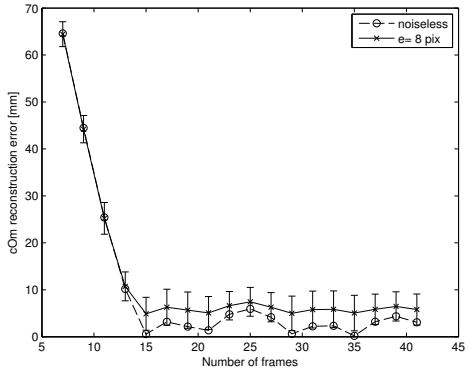

Fig. 6. Reconstruction error vs. number of frames. Noisy and noiseless case.

Figure 6 shows how the mean of the CoM reconstruction error, i.e. the bias arising from the translational velocity estimation decreases linearly as the number of frames increases. The mean error then stabilizes, reflecting that the translational velocity estimator disposed of enough frames to correctly describe the translation. The residual error is due to the error made on the symmetry plane, which, by definition, is independent on the motion and the number of frames.

Figure 7 shows how the CoM-to-Centroid distance affects the reconstruction for different values of N_{frames}. Because

TABLE I
EXPERIMENTAL RESULTS

N_{frames}	$\boldsymbol{a}_r$ [mG]	ϵ [mm]
9	29.5	33
9	28.7	76
11	40	22.9
7	40	16.37
5	42.5	54.29

the translational velocity estimator relies on rotated centroids, decreasing that distance brings the centroids closer to the actual CoM, thus, the estimate is closer to the true value.

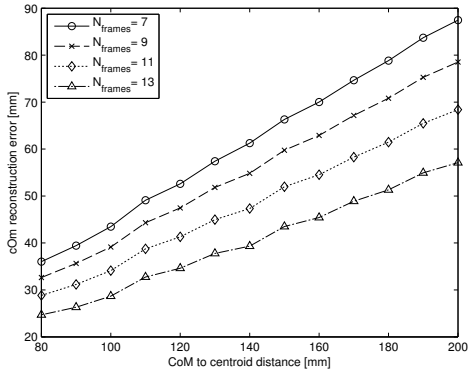

Fig. 7. Reconstruction error vs. CoM-to-Centroid distance

B. Experimental results

It is important to realize that in parabolic flights, the airplane is subject to residual accelerations during the "zero-g" phase, which translates into our referential being non-inertial. From the acceleration signal of the airplane made available to us by Novespace, a measure of the similarity of the experimental conditions with the physical assumptions of our model is proposed. Let G_x, G_y and G_z be respectively the x, y and z acceleration of the airplane during the sequence, expressed in the airplane's reference system. The residual acceleration is:

$$\boldsymbol{a}_r = \left\| \begin{array}{c} E\left[|G_x(k_0-\tau)\dots G_x(k_0+\tau)|\right] \\ E\left[|G_y(k_0-\tau)\dots G_y(k_0+\tau)|\right] \\ E\left[|G_z(k_0-\tau)\dots G_z(k_0+\tau)|\right] \end{array} \right\|$$

Table I shows the reconstruction error obtained during 5 parabolas along with the number of frames N_{frames}.

V. CONCLUSIONS

Because of important residual accelerations occuring during parabolas, only short sequences where considered such that conditions are as close as possible to an inertial reference system. Our motion-based model could be improved to account for those accelerations, thus allowing longer sequences and smaller reconstruction errors. Among the 5 parabolas dedicated to the experiment, 5 sequences of 5 to 9 frames (1-2 seconds) have been retained. The corresponding errors are indeed reasonably close to what has been predicted via simulation.

The motion-based method is intended to be applied to human subjects. Indeed, weightless conditions are known to cause a decrease in the blood concentration gradient, causing the CoM to be shifted towards the head compared with 1-g conditions [6]. The simulations suggest that to improve the accuracy, the centroid should be taken close to the actual CoM. A good a priori would be a measurement at 1-g, which can be obtained in two different ways: Through a biomechanical modeling approach based on body segment kinematics [7], or with a simple force sensor based apparatus.

REFERENCES

[1] B. Atcheson, F. Heide, and W. Heidrich, "Caltag: High precision fiducial markers for camera calibration." in *VMV*, R. Koch, A. Kolb, and C. Rezk-Salama, Eds. Eurographics Association, 2010, pp. 41–48. [Online]. Available: http://dblp.uni-trier.de/db/conf/vmv/vmv2010.html#AtchesonHH10

[2] Z. Zhang, "A flexible new technique for camera calibration," vol. 22, no. 11, pp. 1330–1334, nov 2000.

[3] T. Huang and A. Netravali, "Motion and structure from feature correspondences: A review," *Proceeding of the IEEE*, vol. 82, no. 2, pp. 252–268, 1994.

[4] K. Arun, T. Huang, and S. Blostein, "Least-squares fitting of two 3-d point sets," vol. 9, no. 5, pp. 698–700, Nov. 1987.

[5] M. Moakher, "Means and averaging in the group of rotations," *SIAM J. Matrix Anal. Appl.*, vol. 24, no. 1, pp. 1–16, Jan. 2002. [Online]. Available: http://dx.doi.org/10.1137/S0895479801383877

[6] W. E. Thornton, W. Hoffler, and Rummel, "Anthropometric changes and fluid shifts," in *Biomedical Results from Skylab*, ser. NASA Special Publication, R. S. Johnston and L. F. Dietlein, Eds., vol. 377, 1977, p. 330.

[7] C. Casellato, M. Tagliabue, A. Pedrocchi, C. Papaxanthis, G. Ferrigno, and T. Pozzo, "Reaching while standing in weightlessness: a new postural solution to oversimplify movement control," *Experimental Brain Research*, vol. 216, no. 2, pp. 203–215, 2011.